Captopril treatment during development alleviates mechanically induced aortic remodeling in newborn elastin knockout mice

Jungsil Kim[1], Austin J. Cocciolone[2], Marius C. Staiculescu[1], Robert P. Mecham[3], and Jessica E. Wagenseil[1]

Departments of [1]Mechanical Engineering and Materials Science, [2]Biomedical Engineering, and [3]Cell Biology and Physiology, Washington University, St. Louis, MO

Corresponding Author

Jessica E. Wagenseil, D.Sc.

Department of Mechanical Engineering and Materials Science

Washington University

One Brookings Dr., CB 1185

St. Louis, MO 63130

Ph: 314-935-5052, Fax: 314-935-4014

E-mail: jessica.wagenseil@wustl.edu

Abstract

Deposition of elastin and collagen in the aorta correlate with increases in blood pressure and flow during development, suggesting that the aorta adjusts its mechanical properties in response to hemodynamic stresses. Elastin knockout ($Eln^{-/-}$) mice have high blood pressure, pathological remodeling of the aorta, and die soon after birth. We hypothesized that decreasing blood pressure in $Eln^{-/-}$ mice during development may reduce hemodynamic stresses and alleviate pathological remodeling of the aorta. We treated $Eln^{+/+}$ and $Eln^{-/-}$ mice with the anti-hypertensive medication captopril throughout embryonic development and then evaluated left ventricular (LV) pressure and aortic remodeling at birth. We found that captopril treatment decreased $Eln^{-/-}$ LV pressure to values near $Eln^{+/+}$ mice and alleviated the wall thickening and changes in mechanical behavior observed in untreated $Eln^{-/-}$ aorta. The changes in thickness and mechanical behavior in captopril-treated $Eln^{-/-}$ aorta were not due to alterations in measured elastin or collagen amounts, but may have been caused by alterations in smooth muscle cell (SMC) properties. We used a constitutive model to understand how changes in stress contributions of each wall component could explain the observed changes in composite mechanical behavior. Our modeling results show that alterations in the collagen natural configuration and SMC properties in the absence of elastin may explain untreated $Eln^{-/-}$ aortic behavior and that partial rescue of the SMC properties may account for captopril-treated $Eln^{-/-}$ aortic behavior.

Keywords

Elastin; extracellular matrix; arterial mechanics; arterial development; arterial remodeling; captopril; angiotensin-converting enzyme; angiotensin II

1. Introduction

During aortic development, hemodynamic forces, such as blood pressure and flow, increase concurrently with extracellular matrix (ECM) deposition (Wagenseil and Mecham 2009). ECM proteins, including elastin and collagen, provide elasticity and strength for proper cardiovascular function. When the balance of ECM proteins is upset, such as in genetic mutations that alter the amount or organization of ECM components, mechanical behavior of the aortic wall is changed, leading to altered mechanical stimuli on the smooth muscle cells (SMCs) within the wall. Pathological adaptation to these changes can lead to disease (Humphrey et al. 2014).

Supravalvular aortic stenosis (SVAS) is a genetic disease associated with elastin mutations and functional elastin haploinsufficiency (Li et al. 1997). The cardiovascular manifestation is a narrowed aortic lumen that increases the risk for sudden cardiac death (Wessel et al. 1994). Elastin knockout ($Eln^{-/-}$) mice represent a severe model of SVAS that do not survive beyond birth (Li et al. 1998). $Eln^{-/-}$ mice have hypertension and the aorta is characterized by smooth muscle cell (SMC) overproliferation, luminal narrowing, and increased stiffness (Li et al. 1998; Wagenseil et al. 2009), which are all similar to the human disease phenotype. Previous studies on $Eln^{-/-}$ mice at embryonic day (E) 18 and postnatal (P) day 1, demonstrate that increased aortic stiffness occurs first (at E18) (Wagenseil et al. 2010), followed by increased blood pressure, SMC overproliferation, and additional wall remodeling (at P1) (Wagenseil et al. 2009), suggesting that increased aortic stiffness due to the absence of elastin may be the initiating signal in downstream pathological events (Cheng and Wagenseil 2012).

As there are not yet any pharmaceutical approaches to increase the amounts of crosslinked elastin within the arterial wall in developing mice (Knutsen et al. 2018), we reasoned that pharmaceutically inhibiting the resulting increase in blood pressure may alleviate the additional wall remodeling observed in $Eln^{-/-}$ aorta and limit the pathological effects of elastin insufficiency. We chose captopril, an angiotensin converting enzyme (ACE) inhibitor that has been shown to lower blood pressure in maturing mice (Huang et al. 2013) as our anti-hypertensive agent. We treated pregnant dams with or without captopril and then evaluated blood pressure and aortic remodeling, gene expression, and mechanical behavior in the newborn pups. We used a constitutive model to understand how the absence of elastin and resulting changes in collagen and SMC behavior could explain the resulting composite mechanical behavior of the

aortic wall. Our results show that captopril-treatment during development alleviates mechanically induced aortic remodeling in newborn *Eln*$^{-/-}$ mice. We suggest future research on blood pressure regulation as a treatment option to manipulate developmental aortic remodeling.

2. Methods

2.1 Animals and anti-hypertensive treatment

Eln$^{+/-}$ mice (Li et al. 1998) were bred to produce one day old *Eln*$^{-/-}$ and *Eln*$^{+/+}$ pups. Pregnant dams were treated with captopril, an anti-hypertensive that works through ACE inhibition, in drinking water (0.075 g/L) (Huang et al. 2013) or left untreated. All pups were sacrificed within 24 hours after birth by thoracotomy under 2.5% isoflurane or CO_2 inhalation. Ascending aortic segments from the root to the brachiocephalic artery were used for all aortic studies. Animals were used for blood pressure (N = 7 – 9 per group), protein quantification (N = 3 per pooled group of 5 samples), mRNA expression (n= 3 per pooled group of 8 – 10 samples for *Agtr1a* and *Agtr2*, n = 5 – 6 per group for all other genes), histology and image analysis (N = 6 – 8 per group), aortic dimensions (N = 8 – 15 per group), and mechanical testing (N = 5 – 8 per group). Sex of the animals was not determined. All animal protocols were approved by the Institutional Animal Care and Use Committee at Washington University.

2.2 Left ventricular blood pressure measurement

Newborn pups were anesthetized with 1.5% isoflurane. Body temperature was maintained with a heated stage and radiant lighting. Left ventricular (LV) pressure was measured using a fluid-filled 30G needle under ultrasound guidance (Vevo 2100, Visualsonics), as previously described (Le et al. 2012). The systolic LV pressure was calculated from the mean LV pressure, assuming that the LV diastolic pressure was zero.

2.3 Protein quantification

Five aortic segments per group were pooled and used to measure desmosine (an elastin-specific crosslink), hydroxyproline (an amino acid abundant in collagen), and most amino acids (total protein) as described in Kim et al. (2017). Aortic segments were stored at -80°C and then processed as a batch. Samples were hydrolyzed in 6 N HCl, dried, resuspended in ultrapure water, and stored at -20°C until use. Desmosine was measured through a competitive ELISA

(Cheng et al. 2013). Hydroxyproline was measured through a Chloramine T reaction (Jamall et al. 1981). Total protein was measured through a ninhydrin assay (Starcher 2001). Desmosine and hydroxyproline amounts were normalized to total protein for each group.

2.4 mRNA expression

The expression of *Agtr1a* and *Agtr2*, the main angiotensin II (Ang II) receptor genes in the adult mouse aorta (Burson et al. 1994; Habashi et al. 2011), were measured to determine changes in expression of Ang II signaling genes resulting from captopril treatment. Additionally, the expression of *Mki67* was measured as a marker of cell proliferation (Scholzen and Gerdes 2000) and *Acta2*, *Cnn1*, *Myh11*, *Smtn*, and *Tagln* were measured as markers of SMC phenotype (Rensen et al. 2007). Aortic segments were flash-frozen in liquid nitrogen and stored at -80° until use. For *Agtr1a* and *Agtr2*, 8 – 10 samples were pooled and three pooled samples were used for each group. Total RNA was extracted using a Bullet Blender (Next Advance) tissue homogenizer and the RNeasy Plus Mini Kit (Qiagen). For all other genes, a TissueLyser LT (Qiagen) was used for tissue homogenization and TRIzol Reagent (Invitrogen) for total RNA extraction, which provided a higher yield and did not require pooling of samples. For these genes, 5 – 6 aortic samples were used per group. Reverse transcription was performed using the High Capacity cDNA Reverse Transcription Kit (Applied Biosystems) and 180 ng of total RNA. qPCR was performed with TaqMan Fast Advanced Master Mix (Applied Biosystems) on a QuantStudio 12k machine and analyzed with accompanying software (Applied Biosystems). All experiments were run in triplicate using 2 µl (*Agtr1a and Agtr2*) or 1.2 µl (all other genes) of cDNA in a total volume of 20 µl. Mean C_t of each replicate was normalized to the average of β-2 microglobulin (β2M). Primers were Taqman Gene Expression Assays (Applied Biosystems). Fold change was calculated via the $2^{-\Delta\Delta CT}$ method.

2.5 Histology and image analysis

Aortic segments were dissected, fixed in 10% formalin for 24 hours, and then transferred to 70% ethanol. They were sequentially dehydrated, embedded in paraffin, and cut into 5 µm sections. The sections were stained with hematoxylin and eosin (H&E) and imaged for general cellular morphology.

Color H&E images were converted to grayscale and manually thresholded to highlight cell nuclei. Three regions of the wall that showed a clear cross-section were outlined for each image and cell nuclei were counted using Fiji software (NIH). Cell density was determined by dividing the total nuclei count by the total outlined area for each aortic section. Cell shape was determined using the "Analyze Particles" macro in Fiji for the entire thresholded aortic section. Roundness (4*area/(π*major_axis^2) of the fitted ellipse for each cell nucleus (varying from 257 – 1029 nuclei per image) was calculated. Roundness is the inverse of the aspect ratio and values vary from 0 (line) to 1 (circle). Roundness measurements were combined to generate a total histogram for each group.

2.6 Aortic dimensions and circumferential residual strain

An image was taken with a digital camera connected to a dissecting microscope to measure the length of the ascending aorta *in vivo*. After mechanical testing each aortic segment was placed in physiologic saline solution, cut into 150- to 250-μm thick rings, and imaged to obtain the unloaded diameter and thickness. A radial cut was then made in each ring to determine the residual strain as measured by the opening angle (Chuong and Fung 1986).

2.7 Mechanical testing and data analysis

Aortic segments were dissected and stored at 4°C in physiologic saline solution for up to 3 days before testing (Amin et al. 2011). Passive inflation tests were performed using a Myograph 110P (Danish Myotechnology), as previously described (Kim et al. 2017). The aorta was mounted on custom-designed stainless steel cannulae in a 37°C physiologic saline solution bath with 7-0 silk suture. The unloaded length of the aorta from suture to suture was measured with a caliper. The aorta was extended in the longitudinal direction to the approximate *in vivo* stretch ratio ($\lambda_z = 1.1$) (Kim et al. 2015) and preconditioning cycles were performed until the aorta exhibited repeated behavior for multiple pressurization cycles. The aorta was then pressurized from 0 to 60 mmHg in 5 mmHg step increments, holding for 8 seconds at each step. Three of these cycles were performed while recording outer diameter and lumen pressure at 2 Hz. Average data for each pressure step were determined by averaging all points within ± 1 mmHg of the target pressure. Due to collapse of the aorta at 0 mmHg, data between 5- and 60 mmHg were used for analysis.

Data from the last inflation cycle were used for further analyses. The mean circumferential stretch (λ_θ) at each pressure step was calculated by,

$$\lambda_\theta = \frac{1}{2}\left(\frac{r_i}{R_i} + \frac{r_o}{R_o}\right), \quad \text{Eqn. 1}$$

where r is the loaded radius, R is the unloaded radius and subscripts i and o indicate inner and outer dimensions, respectively. The deformed inner radius was calculated assuming incompressibility (Faury et al. 1999). The mean circumferential stress (σ_θ) at each pressure step was calculated by,

$$\sigma_\theta = \frac{\mathrm{Pr}_i}{r_o - r_i}, \quad \text{Eqn. 2}$$

where P is the applied pressure. The stress-stretch curves were fit to,

$$\sigma_\theta = b_1 + b_2 \exp\left(\frac{\lambda_\theta^{\,b_3}}{b_4}\right), \quad \text{Eqn. 3}$$

where b_i are constants determined by regression in Matlab (Mathworks) (Staiculescu et al. 2017). The tangent physiologic modulus (E_{phys}) was calculated by,

$$E_{phys} = \left.\frac{\partial \sigma_\theta}{\partial \lambda_\theta}\right|_{P=P_{phys}}, \quad \text{Eqn. 4}$$

where P_{phys} = average LV pressure for each group. Any aortic segments that had leaks or did not show repeated behavior for multiple pressurization cycles were excluded from the mechanical testing data, but were used for unloaded dimension and residual strain measurements.

2.8 Constitutive modeling

Constitutive modeling followed previous approaches (Aars 1971; Gleason et al. 2004; Wagenseil 2011). The aortic wall was modeled as a constrained mixture where the stretch ratios for the entire mixture were calculated by Eqn. 1 above for the circumferential direction and by Eqn. 5 below for the axial direction,

$$\lambda_z = \frac{l}{L}, \quad \text{Eqn. 5}$$

where l is the in vivo length and L is the unloaded length. Radial stretch was calculated by incompressibility. It was assumed that each component has a natural configuration in the unloaded state (λ_{i0}) so that the actual stretch ratio of each component in the mixture can be calculated by,

$$\lambda_i^n = \lambda_{i0}^n * \lambda_i \ , \qquad \text{Eqn. 6}$$

where $i = r, \theta,$ or z for the radial, circumferential, and axial directions, respectively, and n represents elastin (e), collagen (c), or SMCs (m) (Fig. 1).

The total stress in each direction (σ_i^{total}) is the sum of each constituent's stress (σ_i^n) multiplied by its volume fraction (ϕ^n),

$$\sigma_i^{total} = \sum_n \phi^n \sigma_i^n \ , \qquad \text{Eqn. 7}$$

Constituent stresses were calculated in the absence of shear and assuming incompressibility. Elastin was considered an isotropic, neo-Hookean solid (Gleason et al. 2004),

$$\sigma_\theta^e(\lambda_\theta^e, \lambda_z^e) = 2\lambda_\theta^e b_1 \left(1 - \frac{1}{\lambda_\theta^{e^4} \lambda_z^{e^2}}\right), \qquad \sigma_z^e(\lambda_\theta^e, \lambda_z^e) = 2\lambda_z^e b_1 \left(1 - \frac{1}{\lambda_\theta^{e^2} \lambda_z^{e^4}}\right), \qquad \text{Eqns. 8a, b}$$

where b_1 is a material constant. Collagen was modeled as a Fung-type, transversely isotropic material with z as the preferred direction (Gleason et al. 2004),

$$\sigma_\theta^c(\lambda_\theta^c, \lambda_z^c) = 2\lambda_\theta^c b_2 b_3 \left(1 - \frac{1}{\lambda_\theta^{c^4} \lambda_z^{c^2}}\right) \exp(Q^c(\lambda_\theta^c, \lambda_z^c)) \ , \qquad \text{Eqn. 9a}$$

$$\sigma_z^c(\lambda_\theta^c, \lambda_z^c) = 2\lambda_\theta^c b_2 \left[b_3 \left(1 - \frac{1}{\lambda_\theta^{c^2} \lambda_z^{c^4}}\right) + 2b_4 \left(\lambda_z^{c^2} - 1\right) \right] \exp(Q^c(\lambda_\theta^c, \lambda_z^c)) \ , \qquad \text{Eqn. 9b}$$

$$\text{with } Q^c(\lambda_\theta^c, \lambda_z^c) = b_3 \left(\lambda_\theta^{c^2} + \lambda_z^{c^2} + \frac{1}{\lambda_\theta^{c^2} \lambda_z^{c^2}} - 3 \right) + b_4 \left(\lambda_z^{c^2} - 1\right)^2 , \qquad \text{Eqn. 9c}$$

where $b_2 - b_4$ are material constants. Passive SMCs were modeled as a transversely isotropic material with a linear term and an exponential term in the θ direction (Gleason et al. 2004),

$$\sigma_{\theta,pas}^m(\lambda_\theta^m, \lambda_z^m) = 2\lambda_\theta^{m^2} \left[b_5 \left(1 - \frac{1}{\lambda_\theta^{m^4} \lambda_z^{m^2}}\right) + 2b_6 b_7 \left(\lambda_\theta^{m^2} - 1\right) \right] \exp(Q^m(\lambda_\theta^m)) \ , \qquad \text{Eqn. 10a}$$

$$\text{with } Q^m(\lambda_\theta^m) = b_7 \left(\lambda_\theta^{m^2} - 1\right)^2 , \qquad \text{Eqn. 10b}$$

$$\sigma^{m}_{z,pas}(\lambda^{m}_{\theta},\lambda^{m}_{z}) = 2\lambda^{m^2}_{z} b_5 \left(1 - \frac{1}{\lambda^{m^2}_{\theta}\lambda^{m^4}_{z}}\right), \qquad \text{Eqn. 10c}$$

where $b_5 - b_7$ are material constants.

Volume fractions were taken from Wagenseil (2011) for a 3-day old mouse aorta, assuming that 75% of the wall is made up of water. Natural configurations were chosen with elastin under slight compression and SMCs in the unloaded state based on observations from the mechanical behavior in Fig. 7 and differences in the timing of elastin deposition and growth in the newborn compared to the adult aorta (Davis 1995; Kelleher et al. 2004). The natural configurations for collagen were calculated from equilibrium of the unloaded mixture. Given the assigned mass fractions and natural configurations, material constants were prescribed based on previous work (Gleason et al. 2004; Wagenseil 2011) and scaled to produce reasonable contributions for each component to approximate the circumferential mechanical behavior of the newborn $Eln^{+/+}$ untreated aorta. For $Eln^{-/-}$ aorta, the elastin volume fraction is zero and water takes up a larger portion of the wall. The collagen natural configurations were then recalculated from equilibrium. $Eln^{-/-}$ aorta was modeled with and without changes to the SMC material constants. The constants used for constitutive modeling are shown in Table 1.

2.9 Statistical analysis

Data are presented as mean ± sd for all figures except the mechanical testing data. Mechanical testing data in Figs. 7A and B are presented as mean ± sem for clarity. Significant differences were determined by analysis of variance (ANOVA), followed by Fisher's LSD for multiple comparisons in Graphpad Prism software. For the cell roundness measurements, visual examination of the histograms showed non-normal distributions, so the Mann-Whitney U test was used to determine mean rank differences between groups in Matlab software. All P values for comparisons between genotype and treatment for $P < 0.1$ are shown in the figures. $P < 0.05$ was considered significant.

3. Results

3.1 Captopril treatment during development decreases LV blood pressure in newborn mice

Captopril treatment decreases LV pressure from 41 to 36 mmHg in $Eln^{-/-}$ mice and from 31 to 27 mmHg in $Eln^{+/+}$ mice (Fig. 2A). Heart rate is 12% higher in captopril treated $Eln^{-/-}$ mice

compared to the untreated group (Fig. 2B), but there is no significant relationship between heart rate and blood pressure ($R^2 = .027$, $P = 0.33$, not shown). The pressure measurements confirm that *Eln*$^{-/-}$ mice have high LV pressure at birth and that captopril treatment during development reduces the LV pressure to the same level as untreated *Eln*$^{+/+}$ mice.

3.2 Captopril treatment decreases wall thickness and opening angle in Eln$^{-/-}$ *aorta*

Captopril treatment during development does not affect the ascending aortic length (Fig. 3A) or unloaded outer diameter (Fig. 3B) of newborn mouse aorta. *Eln*$^{-/-}$ aorta is 40% longer than *Eln*$^{+/+}$, with no significant difference in unloaded outer diameter for the untreated groups. After captopril treatment, *Eln*$^{-/-}$ aorta has a 9% smaller outer diameter than *Eln*$^{+/+}$. *Eln*$^{-/-}$ aorta has increased wall thickness (Fig. 3C) and decreased opening angle (Fig. 2D) compared to *Eln*$^{+/+}$ aorta. Captopril treatment reduces the unloaded wall thickness and opening angle in *Eln*$^{-/-}$ aorta only (Fig. 3C and D).

3.3 Alterations in ECM protein amounts or Ang II receptor gene expression do not account for remodeling of Eln$^{-/-}$ *aortic wall in response to captopril treatment*

Amounts of desmosine and hydroxyproline are not affected by captopril treatment (Fig. 4), indicating that changes in thickness and opening angle in *Eln*$^{-/-}$ aorta are not due to altered deposition of crosslinked elastin or total collagen. As expected, there is no crosslinked elastin present in *Eln*$^{-/-}$ aorta.

Because captopril is an ACE inhibitor, treatment likely stimulates changes in Ang II signaling that may lead to wall remodeling independently of changes in blood pressure. Ang II activity is challenging to measure in newborn mouse aorta, so as a first pass, we measured expression of Ang II receptor genes. We found no significant changes in expression of *Agtr1a* or *Agtr2* in *Eln*$^{-/-}$ aorta in response to captopril treatment (Fig. 5). There is increased expression of *Agtr1a* and *Agtr2* in *Eln*$^{+/+}$ compared to *Eln*$^{-/-}$ in the untreated groups, suggesting reduced expression of Ang II signaling genes in *Eln*$^{-/-}$ aorta at baseline. Expression levels of *Agtr2* are reduced in *Eln*$^{+/+}$ aorta in response to captopril treatment, but are unchanged in *Eln*$^{-/-}$ aorta (Fig. 5B). Together, these results suggest that alterations in expression of Ang II signaling genes are not the primary cause of aortic wall remodeling in *Eln*$^{-/-}$ mice with captopril treatment.

3.4 SMCs appear more organized in $Eln^{-/-}$ aorta with captopril treatment

H&E staining shows an increased number of cells in $Eln^{-/-}$ aorta due to the thicker wall, but there are no significant differences in cell density between groups (Fig. 6). SMC nuclei appear round in cross-sections for untreated $Eln^{-/-}$ aorta, indicating that they are not oriented in the circumferential direction, as they are in $Eln^{+/+}$ aorta. After captopril treatment, the SMCs appear more elongated and circumferentially oriented in $Eln^{-/-}$ aorta. Quantification of nuclear shape confirms that untreated $Eln^{-/-}$ cells are skewed toward higher roundness values than untreated $Eln^{+/+}$ cells and that the $Eln^{-/-}$ distribution shifts toward lower roundness values after captopril treatment (Fig. 6F). Interestingly, captopril treatment has the opposite effect on the shape of $Eln^{+/+}$ nuclei, shifting them to higher roundness values. The changes in SMC organization may lead to the observed reduction in wall thickness and opening angle in $Eln^{-/-}$ aorta in response to captopril treatment and may indicate alterations in SMC phenotype.

3.5 Aortic mechanical behavior is altered in $Eln^{-/-}$ aorta after captopril treatment

We performed mechanical testing to determine how aortic wall remodeling in response to captopril treatment alters structural and material behavior. For untreated and captopril treated groups, $Eln^{-/-}$ aorta becomes more stiff, with little change in outer diameter with increased pressure, at lower diameters than $Eln^{+/+}$ (Fig. 7A). For the untreated group only, $Eln^{-/-}$ aorta is smaller than $Eln^{+/+}$ at pressures between 5 – 25 mmHg. After captopril treatment, the $Eln^{-/-}$ diameter at low pressures is shifted up near $Eln^{+/+}$ levels. The diameter of $Eln^{-/-}$ aorta is significantly different between untreated and captopril treated groups at 5 and 10 mmHg. Pressure-outer diameter data were converted into circumferential stretch-stress data using the measured unloaded dimensions. The untreated $Eln^{-/-}$ curve is shifted to the right of the other groups, indicating higher stretch with lower stress (Fig. 7B). After captopril treatment, the $Eln^{-/-}$ curve is similar to the untreated $Eln^{+/+}$ curve. The tangent physiologic modulus was calculated at the average LV pressure for each group. Captopril treatment increases the modulus of $Eln^{-/-}$ aorta to near $Eln^{+/+}$ levels (Fig. 7C).

3.6 Constitutive modeling suggests altered SMC material properties in $Eln^{-/-}$ aorta after captopril treatment

We used constitutive modeling to understand how component contributions may be altered in *Eln*$^{-/-}$ aorta in response to captopril treatment. The contributions of each component to the composite material behavior of the aortic wall for the baseline model are shown in Fig. 8A with the experimental stretch-stress curve for untreated *Eln*$^{+/+}$ aorta. The prescribed material parameters (Table 1) provide a reasonable approximation of the experimental data and contributions for each wall component. The collagen natural configurations in the *Eln*$^{+/+}$ case were calculated to maintain equilibrium in the unloaded state and are 1.3 in Fig. 8A. To model *Eln*$^{-/-}$ aorta, we assumed that the elastin mass fraction was zero and water takes up a larger fraction of the wall since we did not measure any increases in hydroxyproline amounts (Fig. 4A) or cell density (Fig. 6E). We maintained the material constants for all components and the natural configurations for SMCs. Since elastin is no longer present, the collagen natural configurations have to be recalculated to maintain equilibrium and are equal to 1.0 (Table 1). Fig. 8B shows the resulting total and component stress contributions from the model with no elastin and the experimental data from untreated *Eln*$^{-/-}$ aorta. The model with no elastin shifts the total stress-stretch curves to the right due to the change in collagen natural configuration, but does not quite match the experimental data.

There is evidence that *Eln*$^{-/-}$ SMCs have reduced actin filaments (Karnik et al. 2003) and a decreased passive modulus (Espinosa et al. 2013) compared to *Eln*$^{+/+}$ SMCs. Hence, we reasoned that *Eln*$^{-/-}$ aorta may require altered SMC material constants in our constitutive model. Fig. 8C shows model stresses and component contributions for the same case as Fig. 8B with no elastin, but includes 50% reductions in the linear SMC material constants (Table 1). The model approximates the untreated *Eln*$^{-/-}$ experimental data in Fig. 8C.

After captopril treatment in *Eln*$^{-/-}$ aorta, we have not changed elastin or collagen amounts (Fig. 4) or cell density (Fig. 6E), but we may have altered SMC organization and/or phenotype, as evidenced by the decreased roundness values in the cell orientation histogram (Fig. 6F). Fig. 8D shows the model predictions for the total aortic wall behavior without elastin, but with and without the 50% reduction in the linear SMC material constants. The model without the changes in SMC behavior approximates the experimental data for the captopril treated *Eln*$^{-/-}$ aorta. Our modeling results indicate how complementary changes in collagen natural configurations and SMC material properties can produce mechanical behavior similar to untreated and captopril treated *Eln*$^{-/-}$ aorta.

3.7 SMC gene expression is not significantly different between groups

The constitutive modeling suggests that captopril treatment may rescue SMC material properties in *Eln*$^{-/-}$ aorta. To investigate SMC phenotype changes, we measured gene expression levels of a proliferation marker (*Mki67*) and SMC-specific genes (*Acta2*, *Cnn1*, *Myh11*, *Smtn*, and *Tagln*). There were no significant differences between groups (Fig. 9), indicating no changes in SMC phenotype as linked to expression of these marker genes.

4. Discussion

Developing vessels remodel in response to changes in mechanical stimuli. This was observed by Thoma in 1893 for vasculature in the chick embryo (Clark 1918) and has been supported by studies in the aorta of numerous species including chickens (Espinosa et al. 2018), rats (Gerrity and Cliff 1975), rabbits (Leung et al. 1977), and sheep (Langille 1993). In normal development, remodeling allows the aortic wall to adapt to mechanical demands for optimal cardiovascular function. In abnormal development, the remodeling may exacerbate disease pathology (Humphrey et al. 2014). The remodeling may also be harnessed to manipulate desired outcomes in tissue engineering or disease treatment. For example, culturing tissue engineered arteries under pulsatile pressure increases ECM deposition and burst strength compared to those cultured under static conditions (Niklason et al. 1999). Additionally, the use of anti-hypertensive medication influences the severity of vascular stiffness in Williams Syndrome (Kozel et al. 2014). Williams Syndrome is caused by a contiguous gene deletion that includes the elastin gene and has the same vascular phenotype as SVAS (Pober et al. 2008). In the current study, we show that treating *Eln*$^{-/-}$ mice with captopril during embryonic development lowers blood pressure at birth and induces aortic remodeling that ameliorates the pathologic phenotype associated with the lack of elastin.

We found that newborn, untreated *Eln*$^{-/-}$ mice have 31% higher LV pressure than *Eln*$^{+/+}$, consistent with previous data (Wagenseil et al. 2009). Treating mice with the ACE-inhibitor captopril during embryonic development lowers blood pressure in newborn *Eln*$^{-/-}$ mice to near *Eln*$^{+/+}$ levels. Blood pressure was measured in 5 of the treated *Eln*$^{+/-}$ dams to confirm that captopril was having the desired effect. The systolic pressure of the treated dams was 28% lower than comparable measurements from our laboratory on adult male *Eln*$^{+/-}$ mice (Stoka et al, 2018). In previous studies (Huang et al. 2013), we found a 10 – 15% drop in blood pressure with

captopril treatment in young mice, which is similar to the 12% drop in newborn mice in the current study. The resulting decrease in circumferential wall stress may alleviate the mechanically-mediated increase in wall thickness associated with high blood pressure (Wolinsky 1970), as evidenced by the reduced wall thickness in captopril-treated *Eln*$^{-/-}$ aorta. Captopril-treated *Eln*$^{-/-}$ aorta is still thicker than *Eln*$^{+/+}$ aorta, however, as aortic remodeling is also driven by biochemical signaling in the absence of elastin (Karnik et al. 2003). The decrease in residual strain as measured by opening angle is consistent with reduced hypertensive remodeling in captopril-treated *Eln*$^{-/-}$ aorta (Liu and Fung 1989). Aortic length does not change with captopril treatment in *Eln*$^{-/-}$ aorta, indicating that mechanically-stimulated remodeling in the axial direction is not affected by our chosen anti-hypertensive treatment. Increased wall thickness, decreased opening angle, and increased length in untreated *Eln*$^{-/-}$ aorta compared to *Eln*$^{+/+}$ are similar to previous results in newborn mice (Kim et al. 2017; Wagenseil et al. 2009).

Prior studies investigating remodeling in the developing aorta found alterations in deposition of ECM proteins in response to blood pressure changes (Espinosa et al. 2018; Gerrity and Cliff 1975; Leung et al. 1977). We cannot alter elastin deposition in *Eln*$^{-/-}$ aorta, however, collagen deposition is unchanged in response to reduced elastin levels and changes in blood pressure in the current study and in previous studies on *Eln*$^{+/-}$ (Cheng et al. 2013; Faury et al. 2003) and *Eln*$^{-/-}$ (Kim et al. 2017) mice. Expression of other ECM genes, including non-fibrillar collagens and elastic fiber associated molecules, are altered in *Eln*$^{+/-}$ (Knutsen et al. 2018) and *Eln*$^{-/-}$ (Staiculescu et al. 2018) aorta indicating that the ECM remodeling response is more complicated than previously appreciated.

The response of SMCs to mechanically-induced arterial remodeling includes hypertrophy (Ben Driss et al. 1997) and proliferation (Davis et al. 2005). SMCs overproliferate and are disorganized in *Eln*$^{-/-}$ aorta (Li et al. 1998; Wagenseil et al. 2009). The SMC response is likely due to hypertension in *Eln*$^{-/-}$ mice (Wagenseil et al. 2009), as well as the loss of biochemical elastin signaling (Karnik et al. 2003), and the absence of the physical barrier presented by elastic laminae (Cheng and Wagenseil 2012). We confirmed that cell nuclei are disorganized (rounder) in untreated *Eln*$^{-/-}$ aorta than *Eln*$^{+/+}$ and become more organized in *Eln*$^{-/-}$ aorta after captopril treatment. Despite previous studies showing increased SMC proliferation in late embryonic development (Li et al. 1998) and an increased amount of DNA in the aorta at birth (Wagenseil et al. 2009), *Mki67* expression was not significantly different in untreated *Eln*$^{-/-}$ aorta compared to

Eln$^{+/+}$. It is possible that overproliferation of SMCs is downregulated in *Eln*$^{-/-}$ aorta within 24 hours of birth. Previous work with cultured cells showed reduced expression of SMC marker genes in *Eln*$^{-/-}$ SMCs compared to *Eln*$^{+/+}$ (Espinosa et al. 2013; Karnik et al. 2003), however we found no significant differences in SMC marker gene expression between groups. This may be due to differences between aortic tissue and cultured cells or to the high variability in our SMC gene expression data. The variability may be due to differences in developmental age of the pups at sacrifice (within 24 hours of birth) or individual responses to captopril treatment. Variability was reduced in the analysis of Ang II receptor genes, likely due to pooling of multiple samples, but at the expense of a four-fold increase in required animals. Additional work is needed to further investigate changes in SMC phenotype in response to captopril treatment.

Captopril reduces blood pressure through ACE inhibition and downstream effects on the renin-angiotensin pathway. Ang II is a potent modulator of SMC phenotype and ECM synthesis, hence aortic remodeling in the captopril treated group could be caused by direct effects of Ang II signaling. As measurements of Ang II levels are challenging to obtain in newborn aorta, we quantified mRNA expression of the two main Ang II receptors as an indication of renin-angiotensin signaling activity. We found that both receptors are expressed at lower levels in *Eln*$^{-/-}$ aorta compared to *Eln*$^{+/+}$, suggesting that renin-angiotensin signaling is altered due to the absence of elastin. Ang II receptor expression is not changed by captopril treatment in *Eln*$^{-/-}$ mice, suggesting that alterations in Ang II signaling do not explain the remodeling observed in captopril treated *Eln*$^{-/-}$ aorta. However, receptor gene expression is not a direct measure of Ang II signaling. Previous studies found elevated plasma renin activity (Faury et al. 2003) and augmented Ang II induced vasoconstriction of resistance vessels (Osei-Owusu et al. 2014) in *Eln*$^{+/-}$ mice suggesting hyperactivation of the renin-angiotensin system that may be independent of receptor expression. Future studies with additional anti-hypertensive treatments that act through alternative mechanisms are needed to support our assertion that captopril ameliorates *Eln*$^{-/-}$ aortic remodeling through a reduction in blood pressure.

ECM and SMC amounts, organization, and behavior determine the structural and material properties of the aortic wall. We found that untreated *Eln*$^{-/-}$ aorta has altered structural and material behavior compared to *Eln*$^{+/+}$ aorta, consistent with previous reports (Kim et al. 2017; Wagenseil et al. 2009). Captopril treatment has no effect on *Eln*$^{+/+}$ aorta, but shifts the structural and material behavior of *Eln*$^{-/-}$ aorta toward *Eln*$^{+/+}$ values. The physiologic modulus

values are comparable to previous studies on newborn mouse aorta (Kim et al. 2015; Staiculescu et al. 2017) and are significantly affected by captopril treatment in $Eln^{-/-}$ aorta only. To determine mechanisms that could lead to the observed shifts in mechanical behavior of the composite aortic wall, we employed constitutive modeling. We considered the aortic wall as a constrained mixture of elastin, collagen, and SMCs where each component has a natural configuration (Humphrey and Rajagopal 2002) and we prescribed model constants for illustrative behavior. Our baseline model represents untreated $Eln^{+/+}$ aorta. Elastin has little mechanical contribution in newborn mouse aorta, as the elastic laminae are not yet completely formed (Davis 1995). Despite minimal contributions to the stretch-stress behavior, elastin plays a key mechanical role. We assumed that elastin is slightly compressed in the natural configuration, causing collagen to be stretched to maintain unloaded equilibrium. When elastin is not present in $Eln^{-/-}$ aorta, collagen is no longer stretched in the natural configuration and the collagen contribution to the stretch-stress behavior decreases significantly, mimicking the rightward shift observed experimentally in the untreated $Eln^{-/-}$ stretch-stress curves.

Previous work on adult arteries assumes that elastin is under tension in the natural configuration, which places collagen under compression (Ferruzzi et al. 2011; Fonck et al. 2007; Rachev and Shazly 2019). This set of natural configurations reproduces data on elastase-treated adult arteries where the stress-stretch curves are shifted left toward higher tangent modulus values after elastin degradation, which is the opposite of the untreated $Eln^{-/-}$ mechanical behavior. In adult arteries, it is thought that elastin is under tension in the natural configuration because elastin is deposited during development, does not turnover, and must be stretched as the animal grows (Wagenseil and Mecham 2009). However, elastin production is at a high level in the newborn mouse aorta (Kelleher et al. 2004) and elastin may be compressed at this stage if elastin is being deposited into the elastic laminae at a faster rate than the arterial wall growth.

We assumed that passive SMCs play a large role in the newborn mouse aorta because the ECM is still being deposited (Kelleher et al. 2004). Due to the large SMC contribution, the model stress-stretch curve is not altered enough after the removal of elastin and new natural configurations for collagen to match the experimental data for $Eln^{-/-}$ aorta. We have no experimental evidence for alterations to the collagen material properties, but there is prior evidence for reductions to the passive SMC material properties in $Eln^{-/-}$ aorta. In culture, $Eln^{-/-}$ SMCs have a reduced Young's modulus as measured by atomic force microscopy (Espinosa et

al. 2013), reduced expression of contractile proteins, and limited numbers of actin stress fibers (Karnik et al. 2003). Based on these observations, we reduced the linear SMC material constants by 50% in the model. With reduced SMC material constants, no elastin, and new collagen natural configurations, the model approximates the untreated *Eln*$^{-/-}$ experimental data. With the original SMC material constants, no elastin, and new collagen natural configurations, the model approximates the captopril treated *Eln*$^{-/-}$ experimental data, indicating that changes to the SMC properties alone could explain our results for captopril treated *Eln*$^{-/-}$ aorta.

Our experimental results show that captopril treatment ameliorates *Eln*$^{-/-}$ aortic remodeling and suggest that reducing blood pressure may be a viable treatment option for reducing or delaying pathological aortic remodeling due to elastin insufficiency. Our constitutive model suggests that the observed changes in aortic structural and material properties may be mediated by mechanically-stimulated alterations in SMC phenotype. Anti-hypertensive treatment in utero is not advised in humans due to possible birth defects, however, many children with elastin insufficiency are already prescribed anti-hypertensive medications (Bouchireb et al. 2010). It is possible that anti-hypertensive treatment in childhood would be sufficient to ameliorate some vascular phenotypes in humans with elastin insufficiency. There is evidence that elastin expression continues throughout life in adult human aorta (Fritze et al. 2012), even though elastin expression is turned off in adult mouse aorta (Kelleher et al. 2004), indicating that there may be a longer treatment window in humans than mice for elastin insufficiency. As there are currently no pharmaceutical strategies to increase elastin deposition in developing aorta, pharmaceutical strategies that manipulate aortic remodeling to improve structural and material properties through alternative mechanisms are an encouraging avenue for treatment of genetic elastinopathies.

Limitations and future directions

Sex of the animals was not determined, so sex-dependent variation for the effectiveness of captopril treatment in reducing blood pressure and the effects on the aortic mechanical behavior are unknown. Our conclusions are based on results with a single anti-hypertensive drug. Our results must be tested through additional studies with anti-hypertensives that work through different mechanisms to confirm that the changes are due to decreased blood pressure and not through captopril-specific pathways such as modulation of renin-angiotensin signaling. Captopril

treatment increased heart rate and aortic diameter in $Eln^{-/-}$ mice. These changes would affect the Wormersley number and the pulsatile nature of the blood flow which may have effects on endothelial cell signaling. Endothelial cell changes should be addressed in future research. Our mechanical test data and model are based on the assumption of elastic material behavior and ignore viscoelastic effects. Previous work has shown differences in viscoelastic behavior between $Eln^{+/+}$ and $Eln^{-/-}$ aorta (Kim et al. 2017), which may also be affected by captopril treatment. Our model has several limitations including the prescribed material parameters and natural configurations that must be experimentally determined in future work.

Table 1

Prescribed parameters for constitutive modeling. Natural configurations (Fig. 1) for elastin and SMCs were assumed based on observations from the mechanical behavior and differences in the timing of elastin deposition and growth in the newborn compared to the adult aorta. Collagen values were calculated by equilibrium in the unloaded state. Collagen natural configurations change for the $Eln^{-/-}$ case when elastin is not present. Volume fractions were taken from Wagenseil (2011) for a 3-day old mouse aorta, assuming that 75% of the wall is made up of water. Elastin volume fraction is zero for the $Eln^{-/-}$ case and water takes up a larger portion of the wall. Material properties were scaled from previous work (Gleason et al. 2004; Wagenseil 2011) to approximate the behavior of $Eln^{+/+}$ newborn aorta in the circumferential direction and to provide reasonable contributions for each wall component (Fig. 8A). For the first $Eln^{-/-}$ case, no material properties were changed (Fig. 8B). For the second $Eln^{-/-}$ case, SMC material constants were reduced, as suggested by experimental data (Espinosa et al. 2013; Karnik et al. 2003) (Fig. 8C). Changes compared to the baseline case are highlighted in bold text. e = elastin, c = collagen, m = SMCs. Constants defined in text and equations 6 – 10.

Group, Model Figure	**Natural configurations**	**Volume fractions**	**Material properties**
$Eln^{+/+}$ Baseline, Fig. 8A	$\lambda^e_{\theta 0} = 0.95$, $\lambda^e_{z0} = 0.95$ $\lambda^c_{\theta 0} = 1.31$, $\lambda^c_{z0} = 1.30$ $\lambda^m_{\theta 0} = 1.00$, $\lambda^m_{z0} = 1.00$	$\phi^e = .058$ $\phi^c = .019$ $\phi^m = .173$	b_1 (e) = 5 kPa b_2 (c) = 5 kPa b_3 (c) = 0.5 b_4 (c) = 0.001 b_5 (m) = 8 kPa b_6 (m) = 8 kPa b_7 (m) = 0.05
$Eln^{-/-}$ No elastin, Figs. 8B and 8D	**$\lambda^e_{\theta 0}$ = N/A, λ^e_{z0} = N/A** $\lambda^m_{\theta 0} = 1.00$, $\lambda^m_{z0} = 1.00$ **$\lambda^c_{\theta 0} = 1.00$, $\lambda^c_{z0} = 1.00$**	**$\phi^e = 0$** $\phi^c = .019$ $\phi^m = .173$	**b_1 (e) = N/A** b_2 (c) = 5 kPa b_3 (c) = 0.5 b_4 (c) = 0.001 b_5 (m) = 8 kPa b_6 (m) = 8 kPa

			b_7 (m) = 0.05
Eln$^{-/-}$ No elastin and reduced SMC linear constants, Figs. 8C and 8D	$\boldsymbol{\lambda^e_{\theta 0}}$ **= N/A,** $\boldsymbol{\lambda^e_{z0}}$ **= N/A** $\lambda^m_{\theta 0}$ = 1.00, λ^m_{z0} = 1.00 $\boldsymbol{\lambda^c_{\theta 0}}$ **= 1.00,** $\boldsymbol{\lambda^c_{z0}}$ **= 1.00**	$\boldsymbol{\phi^e}$ **= 0** ϕ^c = .019 ϕ^m = .173	$\boldsymbol{b_1}$ **(e) = N/A** b_2 (c) = 5 kPa b_3 (c) = 0.5 b_4 (c) = 0.001 $\boldsymbol{b_5}$ **(m) = 4 kPa** $\boldsymbol{b_6}$ **(m) = 4 kPa** b_7 (m) = 0.05

Figure Legends

Figure 1. Depiction of the natural configurations ($\lambda^n_{\theta 0}$, λ^n_{z0}) for each component (n = Elastin, Collagen, or SMCs) in the aortic wall. Relationships for the component natural configurations to the component stretch ratios (λ^n_{θ} , λ^n_{z}) and the stretch ratios for the composite mixture (λ_{θ} , λ_{z}) are shown, as defined in Eqn. 6.

Figure 2. LV blood pressure (A) and heart rate (B) in newborn *Eln*$^{-/-}$ and *Eln*$^{+/+}$ mice treated with (Cap) and without (Unt) captopril during development. Each data point represents one animal. Lines are mean ± sd.

Figure 3. Aortic dimensions and residual strain in newborn *Eln*$^{-/-}$ and *Eln*$^{+/+}$ mice treated with (Cap) and without (Unt) captopril during development. In vivo length (A), unloaded outer diameter (B), unloaded thickness (C), and opening angle (D) as a measure of residual strain are shown. Each data point represents one animal. Lines are mean ± sd.

Figure 4. Aortic desmosine (A) and hydroxyproline (B) were measured and normalized to total protein to quantify crosslinked elastin and total collagen amounts, respectively, in newborn *Eln*$^{-/-}$ and *Eln*$^{+/+}$ mice treated with (Cap) and without (Unt) captopril during development. Each data point represents one group of 5 pooled aortic samples. Lines are mean ± sd.

Figure 5. Aortic mRNA levels of *Agtr1a* (A) and *Agtr2* (B) were measured to quantify Ang II signaling in newborn *Eln*$^{-/-}$ and *Eln*$^{+/+}$ mice treated with (Cap) and without (Unt) captopril during development. Values were normalized to *B2M* and then to Unt *Eln*$^{+/+}$ controls. Each data point represents one group of 8 – 10 pooled aortic samples. Lines are mean ± sd.

Figure 6. H&E stained aortic sections of newborn *Eln*$^{-/-}$ and *Eln*$^{+/+}$ mice treated with (Cap) and without (Unt) captopril during development (A – D). Note the circular shape of the SMC nuclei in the Unt *Eln*$^{-/-}$ aorta (white arrow) that is less apparent in the Cap *Eln*$^{-/-}$ aorta. Scale bar = 10 μm. Cell density (E) was quantified by counting cell nuclei in defined areas of the H&E images. Each data point represents one aortic image. Cell shape was quantified by determining the

roundness of the cell nuclei in the entire aortic cross-section (F). Histograms include all cells counted in each group. Unt *Eln*$^{-/-}$ nuclei are significantly more round than Unt *Eln*$^{+/+}$ and Cap *Eln*$^{-/-}$. Cap *Eln*$^{+/+}$ nuclei are significantly more round than Unt *Eln*$^{+/+}$ nuclei. * = P < .05.

Figure 7. Circumferential mechanical behavior of the aorta from newborn *Eln*$^{-/-}$ and *Eln*$^{+/+}$ mice treated with (Cap) and without (Unt) captopril during development. Unt *Eln*$^{-/-}$ aorta has reduced outer diameter compared to Unt *Eln*$^{+/+}$ at pressures between 5 – 25 mmHg ($) (A). The reduced outer diameter in *Eln*$^{-/-}$ aorta is increased at 5 and 10 mmHg after captopril treatment (#). Circumferential stretch-stress behavior shows the rightward shift (arrow) in Unt *Eln*$^{-/-}$ aorta that appears to be rescued with captopril treatment (B). $ = P < 0.05 between Unt *Eln*$^{+/+}$ and *Eln*$^{-/-}$. # = P < 0.05 between Unt *Eln*$^{-/-}$ and Cap *Eln*$^{-/-}$. Data are plotted as mean ± sem and lines are interpolated between measured data points. Tangent physiologic modulus was calculated at the mean LV pressure for each group (C). Each data point represents one aorta and lines are mean ± sd. N = 7 for Unt *Eln*$^{-/-}$, N = 5 for Cap *Eln*$^{-/-}$, N = 8 for Unt *Eln*$^{+/+}$, and N = 8 for Cap *Eln*$^{+/+}$.

Figure 8. Constitutive modeling of the aortic mechanical behavior from newborn *Eln*$^{-/-}$ and *Eln*$^{+/+}$ mice treated with (Cap) and without (Unt) captopril during development. Model parameters are summarized in Table 1. Panels A, B, and C show total model contributions, as well as the contributions of each wall component. Panel A = Baseline model compared to Unt *Eln*$^{+/+}$ experimental data. Panel B = Model with no elastin compared to Unt *Eln*$^{-/-}$ experimental data. Panel C = Model with no elastin and reduced SMC material constants compared to Unt *Eln*$^{-/-}$ experimental data. Panel D = Total model contributions with constants in Panels B and C compared to Unt *Eln*$^{-/-}$ and Cap *Eln*$^{-/-}$ experimental data.

Figure 9. Aortic mRNA levels of *Mki67* (A), *Acta2* (B), *Cnn1* (C), *Myh11* (D), *Smtn* (E), and *Tagln* (F) were measured to quantify proliferation and SMC phenotype in newborn *Eln*$^{-/-}$ and *Eln*$^{+/+}$ mice treated with (Cap) and without (Unt) captopril during development. Values were normalized to *B2M* and then to Unt *Eln*$^{+/+}$ controls. Each data point represents one aortic sample. Lines are mean ± sd.

Funding

This study was partially funded by NSF grant 1662434 (J. Wagenseil), NIH grants HL-115560 (J. Wagenseil), HL-53325 (R. Mecham), and HL-105314 (R. Mecham and J. Wagenseil).

Conflict of Interest

The authors declare that they have no conflict of interest.

References

Aars H (1971) Effects of altered smooth muscle tone on aortic diameter and aortic baroreceptor activity in anesthetized rabbits Circ Res 28:254-262

Amin M, Kunkel AG, Le VP, Wagenseil JE (2011) Effect of storage duration on the mechanical behavior of mouse carotid artery J Biomech Eng 133:071007 doi:10.1115/1.4004415

Ben Driss A, Benessiano J, Poitevin P, Levy BI, Michel JB (1997) Arterial expansive remodeling induced by high flow rates Am J Physiol 272:H851-858

Bouchireb K et al. (2010) Clinical features and management of arterial hypertension in children with Williams-Beuren syndrome Nephrol Dial Transplant 25:434-438 doi:10.1093/ndt/gfp522

Burson JM, Aguilera G, Gross KW, Sigmund CD (1994) Differential expression of angiotensin receptor 1A and 1B in mouse Am J Physiol 267:E260-267 doi:10.1152/ajpendo.1994.267.2.E260

Cheng JK, Stoilov I, Mecham RP, Wagenseil JE (2013) A fiber-based constitutive model predicts changes in amount and organization of matrix proteins with development and disease in the mouse aorta Biomech Model Mechanobiol 12:497-510 doi:10.1007/s10237-012-0420-9

Cheng JK, Wagenseil JE (2012) Extracellular matrix and the mechanics of large artery development Biomech Model Mechanobiol doi:10.1007/s10237-012-0405-8

Chuong CJ, Fung YC (1986) On residual stresses in arteries J Biomech Eng 108:189-192

Clark ER (1918) Studies on the growth of blood-vessels in the tail of the frog larva - by observation and experiment on the living animal American Journal of Anatomy 23:37 - 88

Davis EC (1995) Elastic lamina growth in the developing mouse aorta J Histochem Cytochem 43:1115-1123

Davis NP, Han HC, Wayman B, Vito R (2005) Sustained axial loading lengthens arteries in organ culture Ann Biomed Eng 33:867-877

Espinosa MG, Gardner WS, Bennett L, Sather B, Yanagisawa H, Wagenseil JE (2013) The Effects of Elastic Fiber Protein Insufficiency and Treatment on the Modulus of Arterial Smooth Muscle Cells J Biomech Eng doi:10.1115/1.4026203

Espinosa MG, Taber LA, Wagenseil JE (2018) Reduced embryonic blood flow impacts extracellular matrix deposition in the maturing aorta Developmental dynamics : an official publication of the American Association of Anatomists doi:10.1002/dvdy.24635

Faury G, Maher GM, Li DY, Keating MT, Mecham RP, Boyle WA (1999) Relation between outer and luminal diameter in cannulated arteries Am J Physiol 277:H1745-1753

Faury G et al. (2003) Developmental adaptation of the mouse cardiovascular system to elastin haploinsufficiency J Clin Invest 112:1419-1428

Ferruzzi J, Vorp DA, Humphrey JD (2011) On constitutive descriptors of the biaxial mechanical behaviour of human abdominal aorta and aneurysms J R Soc Interface 8:435-450 doi:10.1098/rsif.2010.0299

Fonck E, Prod'hom G, Roy S, Augsburger L, Rufenacht DA, Stergiopulos N (2007) Effect of elastin degradation on carotid wall mechanics as assessed by a constituent-based biomechanical model Am J Physiol Heart Circ Physiol 292:H2754-2763 doi:10.1152/ajpheart.01108.2006

Fritze O et al. (2012) Age-related changes in the elastic tissue of the human aorta J Vasc Res 49:77-86 doi:10.1159/000331278

Gerrity RG, Cliff WJ (1975) The aortic tunica media of the developing rat. I. Quantitative stereologic and biochemical analysis Lab Invest 32:585-600

Gleason RL, Taber LA, Humphrey JD (2004) A 2-D Model of Flow-Induced Alterations in the Geometry, Structure and Properties of Carotid Arteries J Biomech Eng 126:371-381

Habashi JP et al. (2011) Angiotensin II type 2 receptor signaling attenuates aortic aneurysm in mice through ERK antagonism Science 332:361-365 doi:10.1126/science.1192152

Huang J et al. (2013) Angiotensin-converting enzyme-induced activation of local angiotensin signaling is required for ascending aortic aneurysms in fibulin-4-deficient mice Science translational medicine 5:183ra158, 181-111 doi:10.1126/scitranslmed.3005025

Humphrey JD, Milewicz DM, Tellides G, Schwartz MA (2014) Cell biology. Dysfunctional mechanosensing in aneurysms Science 344:477-479 doi:10.1126/science.1253026

Humphrey JD, Rajagopal KR (2002) A constrained mixture model for growth and remodeling of soft tissues Mathematical Models & Methods in Applied Sciences 12:407-430

Jamall IS, Finelli VN, Que Hee SS (1981) A simple method to determine nanogram levels of 4-hydroxyproline in biological tissues Analytical biochemistry 112:70-75

Karnik SK et al. (2003) A critical role for elastin signaling in vascular morphogenesis and disease Development 130:411-423

Kelleher CM, McLean SE, Mecham RP (2004) Vascular extracellular matrix and aortic development Curr Top Dev Biol 62:153-188

Kim J, Procknow JD, Yanagisawa H, Wagenseil JE (2015) Differences in genetic signaling, and not mechanical properties of the wall, are linked to ascending aortic aneurysms in fibulin-4 knockout mice Am J Physiol Heart Circ Physiol 309:H103-113 doi:10.1152/ajpheart.00178.2015

Kim J, Staiculescu MC, Cocciolone AJ, Yanagisawa H, Mecham RP, Wagenseil JE (2017) Crosslinked elastic fibers are necessary for low energy loss in the ascending aorta J Biomech 61:199-207 doi:10.1016/j.jbiomech.2017.07.011

Knutsen R et al. (2018) Minoxidil improves vascular compliance, restores cerebral blood flow and alters extracellular matrix gene expression in a model of chronic vascular stiffness Am J Physiol Heart Circ Physiol doi:10.1152/ajpheart.00683.2017

Kozel BA et al. (2014) Williams syndrome predisposes to vascular stiffness modified by antihypertensive use and copy number changes in NCF1 Hypertension 63:74-79 doi:10.1161/HYPERTENSIONAHA.113.02087

Langille BL (1993) Remodeling of developing and mature arteries: endothelium, smooth muscle, and matrix J Cardiovasc Pharmacol 21 Suppl 1:S11-17

Le VP, Kovacs A, Wagenseil JE (2012) Measuring left ventricular pressure in late embryonic and neonatal mice Journal of visualized experiments : JoVE doi:10.3791/3756

Leung DY, Glagov S, Mathews MB (1977) Elastin and collagen accumulation in rabbit ascending aorta and pulmonary trunk during postnatal growth. Correlation of cellular synthetic response with medial tension Circ Res 41:316-323

Li DY et al. (1998) Elastin is an essential determinant of arterial morphogenesis Nature 393:276-280

Li DY, Toland AE, Boak BB, Atkinson DL, Ensing GJ, Morris CA, Keating MT (1997) Elastin point mutations cause an obstructive vascular disease, supravalvular aortic stenosis Human molecular genetics 6:1021-1028

Liu SQ, Fung YC (1989) Relationship between hypertension, hypertrophy, and opening angle of zero-stress state of arteries following aortic constriction J Biomech Eng 111:325-335

Niklason LE, Gao J, Abbott WM, Hirschi KK, Houser S, Marini R, Langer R (1999) Functional arteries grown in vitro Science 284:489-493

Osei-Owusu P, Knutsen RH, Kozel BA, Dietrich HH, Blumer KJ, Mecham RP (2014) Altered reactivity of resistance vasculature contributes to hypertension in elastin insufficiency Am J Physiol Heart Circ Physiol 306:H654-666 doi:10.1152/ajpheart.00601.2013

Pober B, Johnson M, Urban Z (2008) Mechanisms and treatment of cardiovascular disease in Williams-Beuren syndrome. J Clin Invest 118:1606-1615 doi:10.1172/JCI35309

Rachev A, Shazly T (2019) A structure-based constitutive model of arterial tissue considering individual natural configurations of elastin and collagen J Mech Behav Biomed Mater 90:61-72 doi:10.1016/j.jmbbm.2018.09.047

Rensen SSM, Doevendans PAFM, van Eys GJJM (2007) Regulation and characteristics of vascular smooth muscle cell phenotypic diversity Netherlands Heart Journal 15:100-108

Scholzen T, Gerdes J (2000) The Ki-67 protein: from the known and the unknown J Cell Physiol 182:311-322 doi:10.1002/(SICI)1097-4652(200003)182:3<311::AID-JCP1>3.0.CO;2-9

Staiculescu MC, Cocciolone A, Procknow J, Kim J, Wagenseil JE (2018) Comparative gene array analyses of severe elastic fiber defects in late embryonic and newborn mouse aorta Physiological genomics doi:10.1152/physiolgenomics.00080.2018

Staiculescu MC, Kim J, Mecham RP, Wagenseil J (2017) Mechanical behavior and matrisome gene expression in aneurysm-prone thoracic aorta of newborn lysyl oxidase knockout

mice Am J Physiol Heart Circ Physiol:ajpheart 00712 02016 doi:10.1152/ajpheart.00712.2016

Starcher B (2001) A ninhydrin-based assay to quantitate the total protein content of tissue samples Analytical biochemistry 292:125-129 doi:10.1006/abio.2001.5050

Wagenseil JE (2011) A constrained mixture model for developing mouse aorta Biomech Model Mechanobiol 10:671-687 doi:10.1007/s10237-010-0265-z

Wagenseil JE, Ciliberto CH, Knutsen RH, Levy MA, Kovacs A, Mecham RP (2009) Reduced vessel elasticity alters cardiovascular structure and function in newborn mice Circ Res 104:1217-1224 doi:10.1161/CIRCRESAHA.108.192054

Wagenseil JE, Ciliberto CH, Knutsen RH, Levy MA, Kovacs A, Mecham RP (2010) The importance of elastin to aortic development in mice Am J Physiol Heart Circ Physiol 299:H257-264 doi:10.1152/ajpheart.00194.2010

Wagenseil JE, Mecham RP (2009) Vascular extracellular matrix and arterial mechanics Physiol Rev 89:957-989 doi:10.1152/physrev.00041.2008

Wessel A, Pankau R, Kececioglu D, Ruschewski W, Bursch JH (1994) Three decades of follow-up of aortic and pulmonary vascular lesions in the Williams-Beuren syndrome Am J Med Genet 52:297-301 doi:10.1002/ajmg.1320520309

Wolinsky H (1970) Response of the rat aortic media to hypertension. Morphological and chemical studies Circ Res 26:507-522

Fig. 1

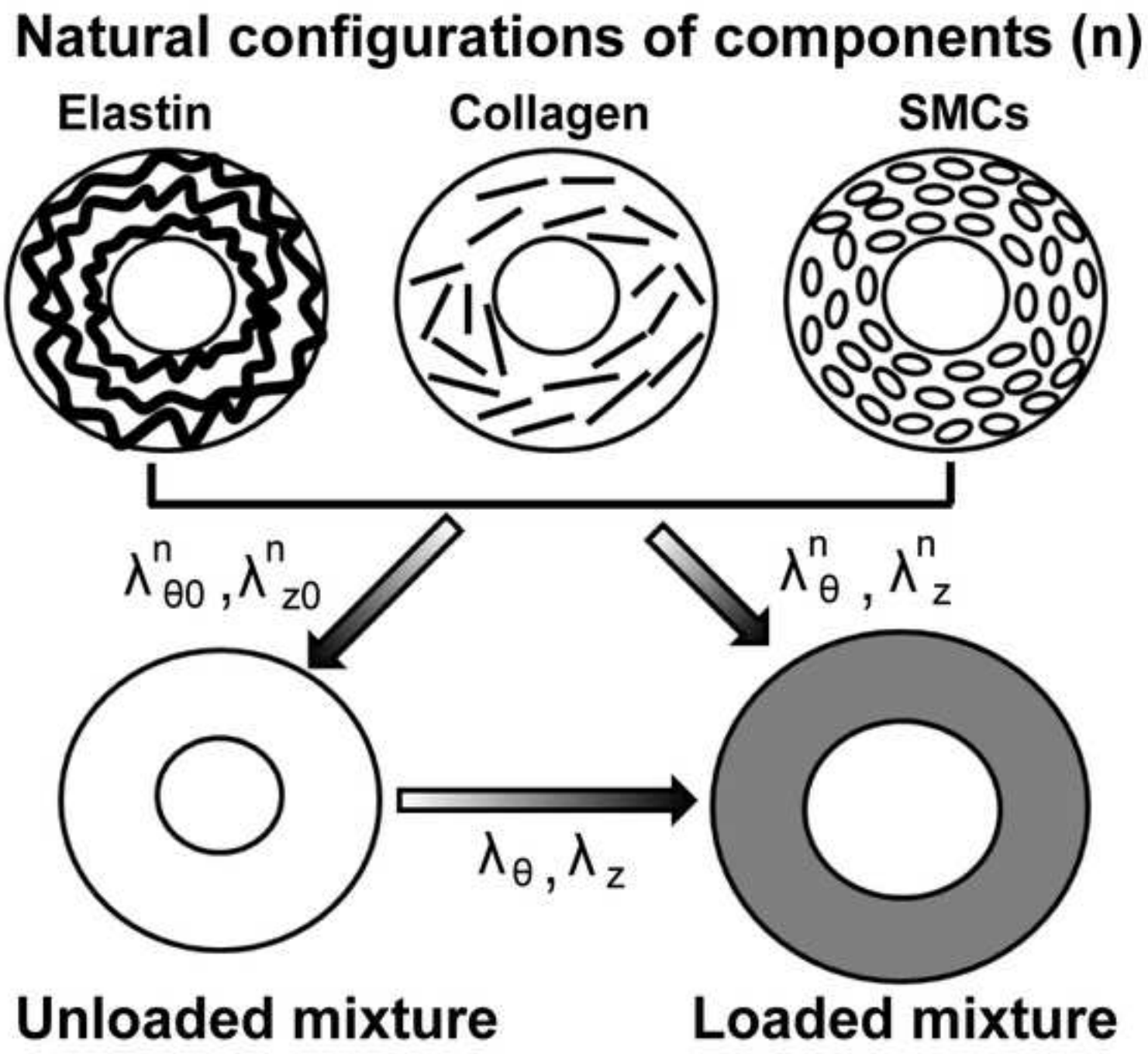

Fig. 2

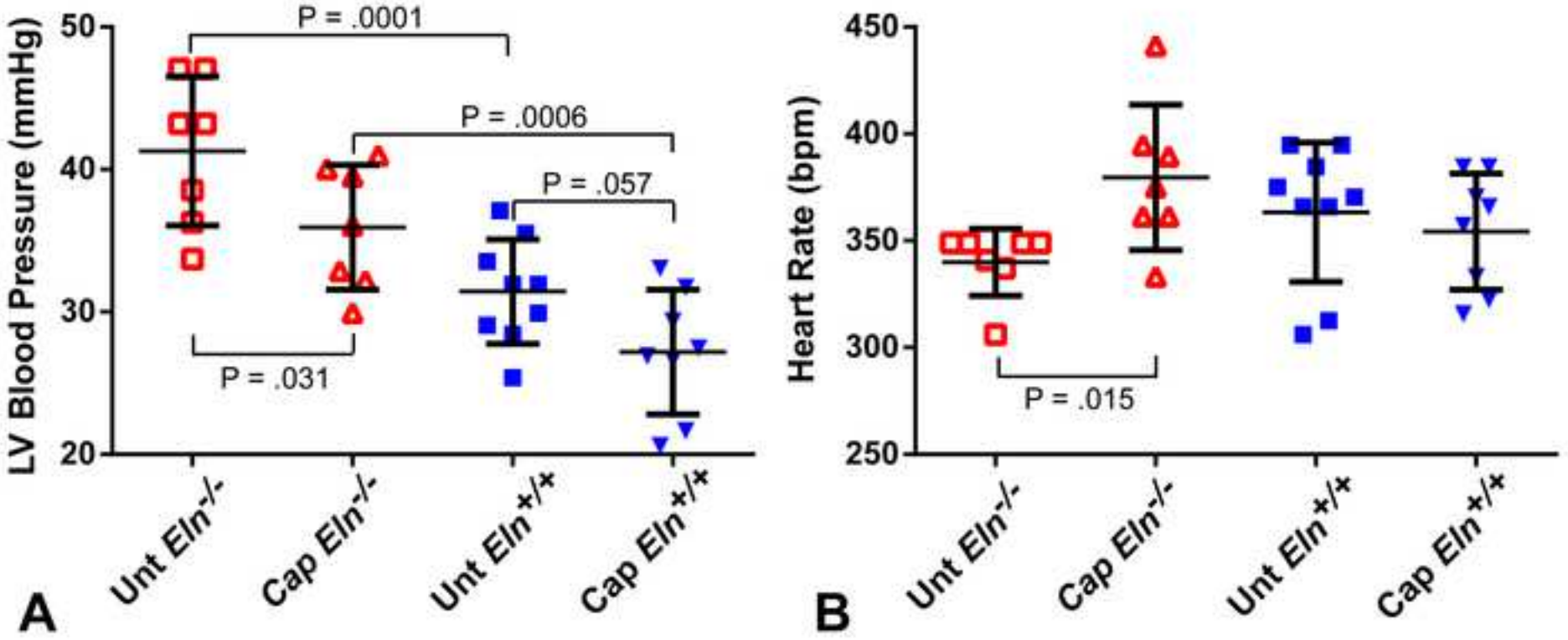

Fig. 3

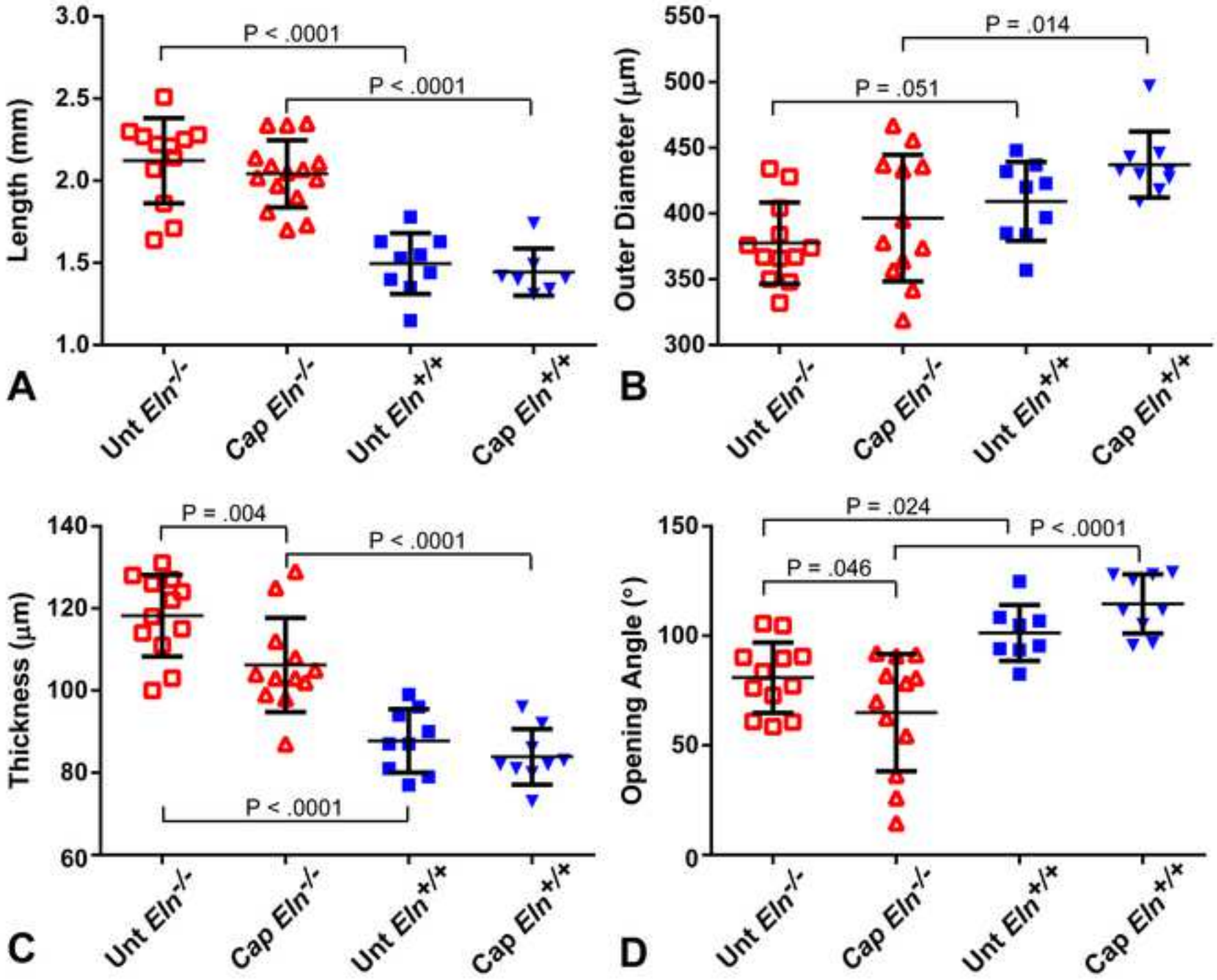

Fig. 4

Click here to access/download;Figure;Fig4_protein_quant_rev1-01.tif

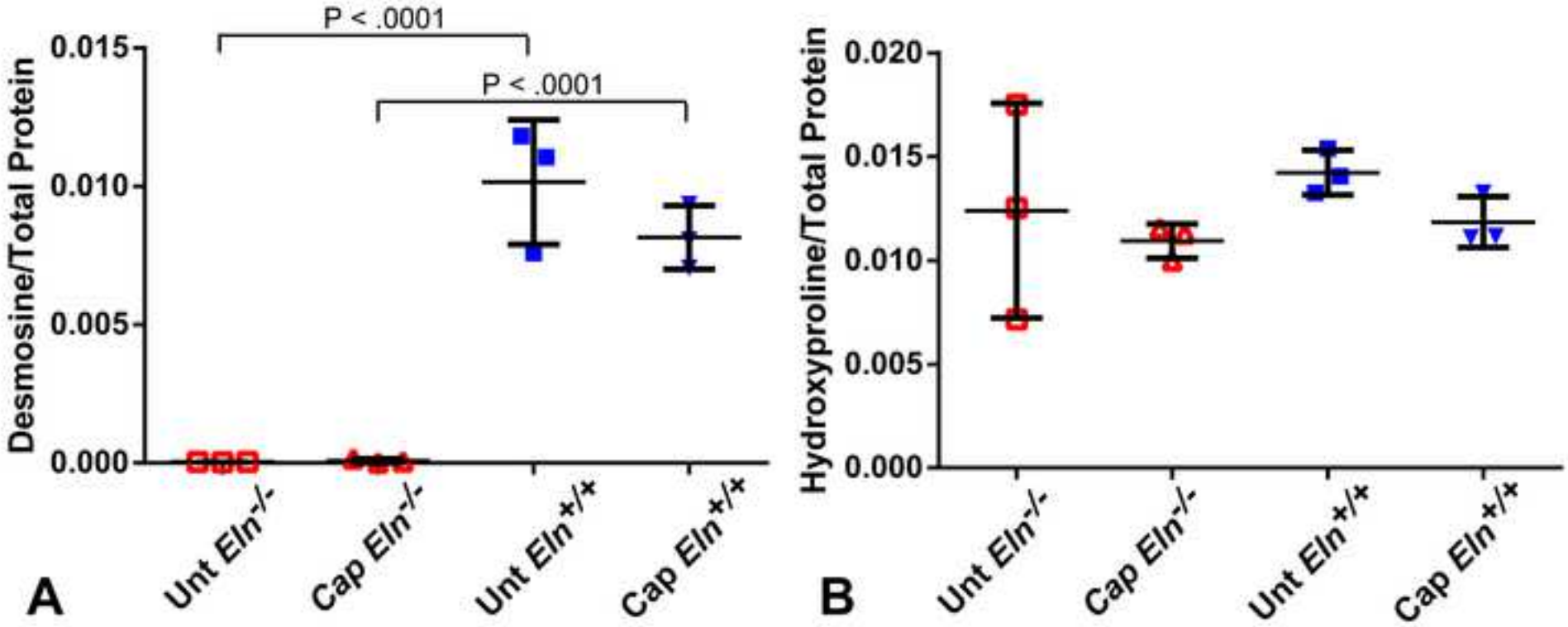

Fig. 5

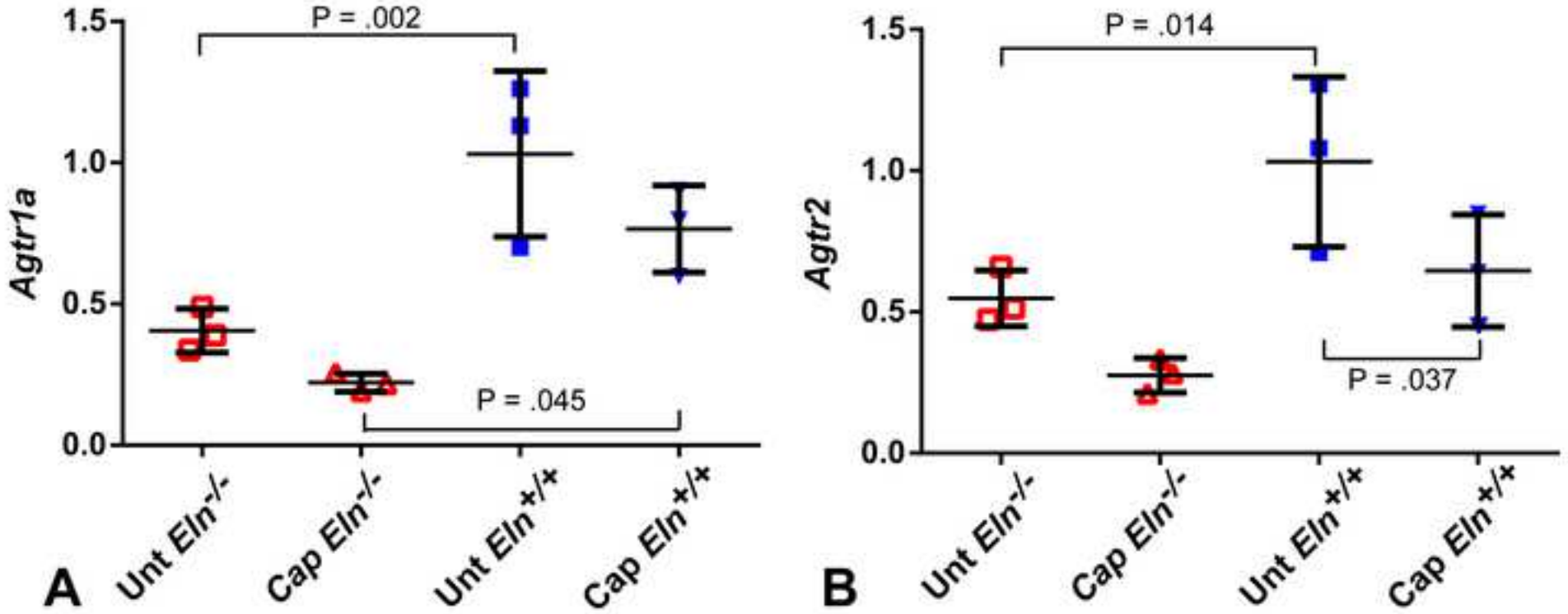

Fig. 6

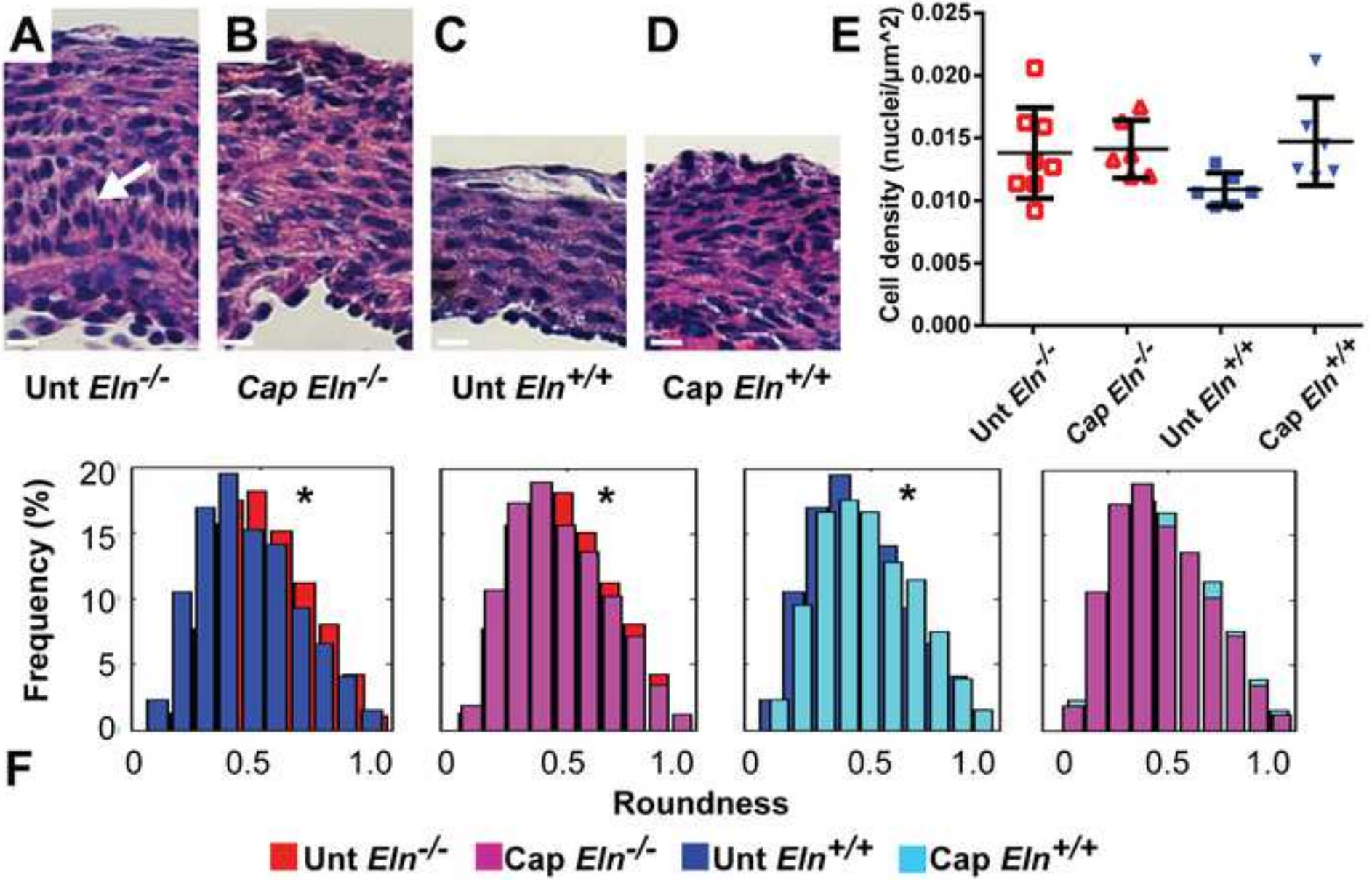

Fig. 7

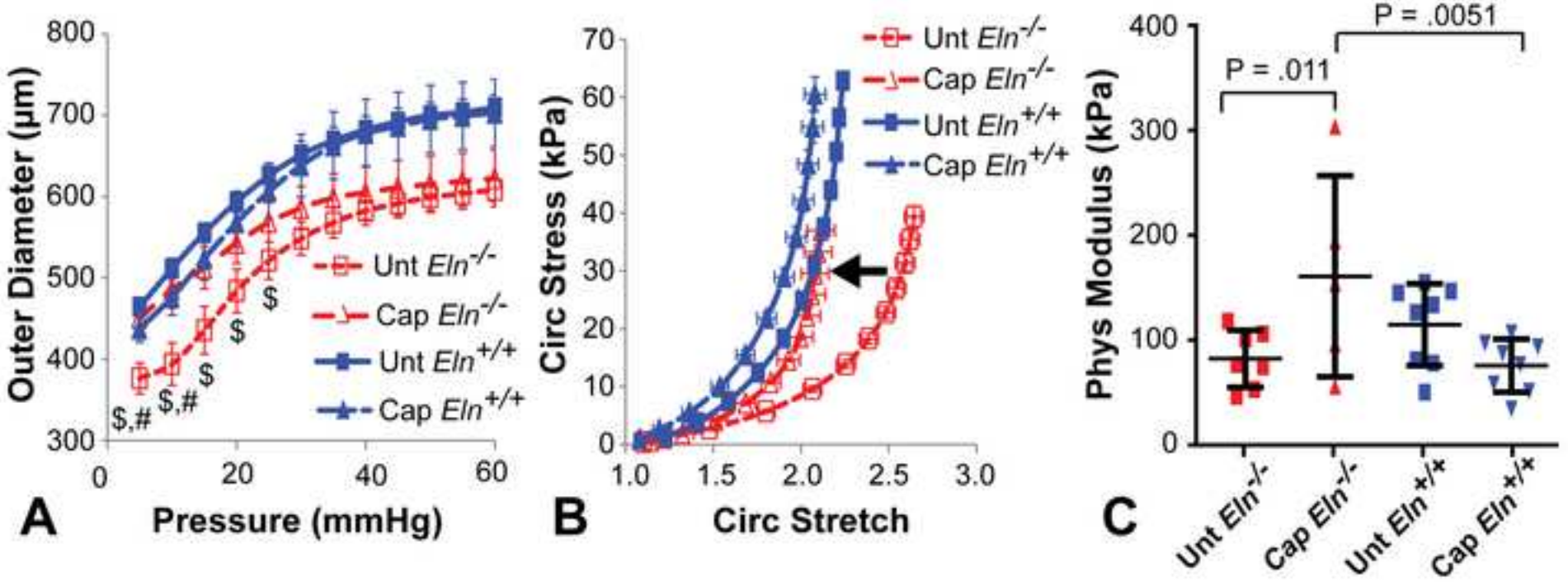

Fig. 8

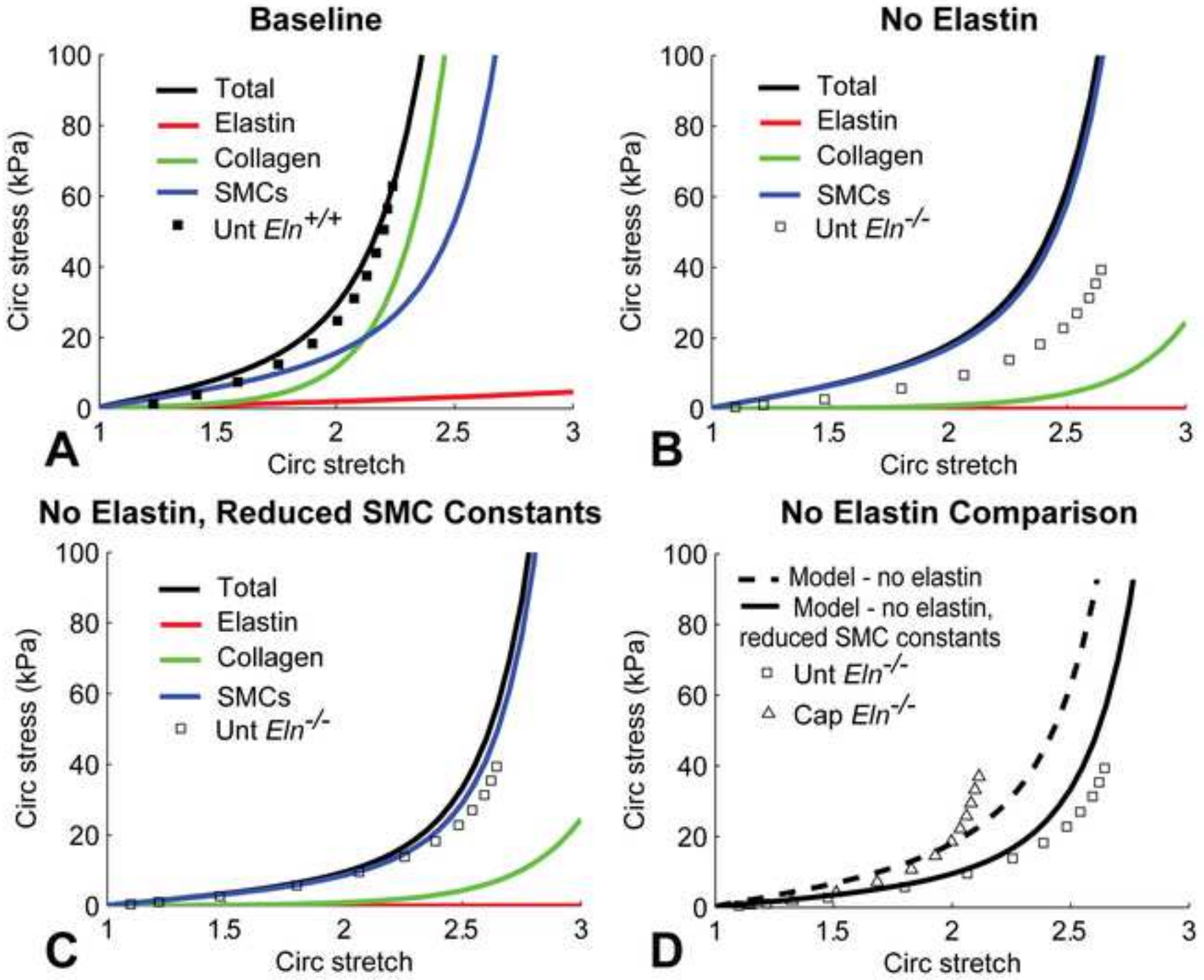

Fig. 9

Click here to access/download;Figure;Fig9_SMC_gene_expression-01.tif